

# CZTS solar cells and the possibility of increasing $V_{OC}$ using evaporated $Al_2O_3$ at the CZTS/CdS interface.

E. Ojeda-Durán<sup>1\*</sup>, K. Monfil-Leyva<sup>1</sup>, J. Andrade-Arvizu<sup>2</sup>, I. Becerril-Romero<sup>2</sup>, Y. Sánchez<sup>2</sup>, R. Fonoll-Rubio<sup>2</sup>, M. Guc<sup>2</sup>, Z. Jehl<sup>2</sup>, J.A. Luna-López<sup>1</sup>, A.L. Muñoz-Zurita<sup>3</sup>, J.A.D. Hernández-de la Luz<sup>1</sup>, V. Izquierdo-Roca<sup>2</sup>, M. Placidi<sup>2</sup>, E. Saucedo<sup>2</sup>.

<sup>1</sup>Research center of Semiconductor Devices, Meritorious University Autonomous of Puebla, 14th south, Col. San Manuel, C.P. 72750, Puebla, Mexico.

<sup>2</sup>Catalonia Institute for Energy Research-IREC, Jardins de les Dones de Negre, 1, 2<sup>a</sup> pl., 08930 Sant Adrià de Besòs, Barcelona, Spain.

<sup>3</sup>Electronics Faculty. Meritorious University Autonomous of Puebla, Av. San Claudio, Col. San Manuel, C.P. 72570, Puebla, Mexico.

\*Corresponding author: [esteban.ojeda@alumno.buap.mx](mailto:esteban.ojeda@alumno.buap.mx)

**ABSTRACT** — We report the effect of an ultra-thin  $Al_2O_3$  layer (down to 3 nm) as interface passivation strategy for the improvement of the performance of  $Cu_2ZnSnS_4/CdS$  based solar cells. After an initial optimization, the  $Al_2O_3$  deposited by thermal evaporation is proved to improve the properties of the p-n junction. The fabricated devices showed an increment in  $V_{oc}$  depending on the composition of the absorber, and an improvement in fill factor (FF) apparently related to the insulation of possible shunt-paths. Also, the impact on other optoelectronic parameters is discussed.

**Index Terms** —  $Cu_2ZnSnS_4$  (CZTS), interface passivation,  $Al_2O_3$ , thermally evaporation.

## 1. INTRODUCTION

Kesterite ( $Cu_2ZnSnS_4$ , CZTS) is an emerging and very promising thin film photovoltaic (PV) material, mainly since it contains exclusively Earth-abundant and low toxicity elements such as Cu, Sn, Zn and S [1]. This is expected to contribute in the future to reduce fabrication costs and allow production at the TW/year level in contrast to the limitation posed by In and Ga scarcity in  $Cu(In,Ga)Se_2$  (CIGS) solar cells [2]. CZTS possesses an excellent light absorption coefficient ( $\sim 10^4 \text{ cm}^{-1}$ ) and a bandgap of  $\sim 1.5$  eV suitable for high efficiency PV devices. The recent record in kesterite solar cells is from Wang *et al.* [3] who reported a 12.6%  $Cu_2ZnSn(S,Se)_4$  (CZTSSe) solar cell, but containing only 25% of S and, still far from the conversion efficiencies reported for more mature thin film technologies like CdTe and CIGS [4]. In the case of the pure sulfide compound, efficiency losses are supposed to be partially related, to possible recombination at the interfaces. This recombination is nominally, between the CZTS absorber and the  $MoS_2$  at the Mo-back contact; and between the CZTS absorber and the CdS-buffer layer [5]. To solve the first problem Yan *et al.* [6] reported the use of  $Al_2O_3$  to avoid the growth of  $MoS_2$ , obtaining an efficiency of 11%. On the other hand, F. Zhou *et al.* [7] reported the use of a thin layer of carbon between Mo and CZTS absorber to increase the  $J_{sc}$ . H. Cui *et al.* [8] showed the use of thin layer of silver ( $\sim 20$  nm) in Mo/CZTS interface, directly increasing the efficiency.

Over other relevant interface (CZTS/CdS), alternative approaches using  $SnO_2$  [9] or using  $Al_2O_3$  deposited by ALD [10], have been reported. Their conclusions pointed towards being hydrogen rather than  $Al_2O_3$  the potential cause of the observed defect passivation. Similarly, H. Xie *et al.* [11] investigated the chemical deposition of  $Al(OH)_3$  to passivate the surface of CZTSSe observing a reduction in the recombination at the CZTSSe/CdS interface, with an improvement in the shunt resistance. The authors also demonstrated an epitaxial relationship of  $Al(OH)_3$  with kesterite and CdS, corroborating an effective interface passivation with this

chemical approach. On the other hand, Erkan *et al.* [12] deposited 1 nm of Al<sub>2</sub>O<sub>3</sub> by ALD, between the CZTSSe absorber and CdS buffer interface. They showed that this approach reduces the density of acceptor-like states at the heterojunction observing in consequence less interface recombination, and improved V<sub>oc</sub>. In the same way, Lee *et al.* [13] deposited 1 nm of Al<sub>2</sub>O<sub>3</sub> on CZTS/CdS and replaced the ZnO film by 10 nm of Al<sub>2</sub>O<sub>3</sub>. They evidenced that the Al signal persists throughout the film, indicating that this layer may also passivate pinholes and grain boundaries. In Table I a summary of passivated interfaces on kesterite solar cells is shown.

TABLE I. SUMMARY OF PASSIVATED INTERFACES ON KESTERITE SOLAR CELLS.

Material	Deposition	Interface	Jsc (mA/cm <sup>2</sup> )	Voc (mV)	Ref.
Al <sub>2</sub> O <sub>3</sub>	ALD	Mo/CZTS	21.7	730	[6]
Carbon	Evaporation	Mo/CZTS	16.9	560	[7]
Ag	Evaporation	Mo/CZTS	15.0	597	[8]
SnO <sub>2</sub>	SILAR	CZTS/CdS	20.5	657	[9]
Al <sub>2</sub> O <sub>3</sub>	ALD	CZTS/CdS	20.1	627	[10]
Al(OH) <sub>3</sub>	Chemical deposition	CZTSSe/CdS	25.6	453	[11]
Al <sub>2</sub> O <sub>3</sub>	ALD	CZTSSe/CdS	13.8	336	[12]
Al <sub>2</sub> O <sub>3</sub>	ALD	CZTS/CdS	32.1	515	[13]

All these works revealed the relevance of CZTS and CZTSSe interface passivation, but with the inherent doubt if such passivation is attributed to either the presence of hydrogen in the system, due to the oxide, or a combination of both. This is due to the use of H<sub>2</sub>O vapor and Trimethyl-aluminium (TMA) in the ALD systems to obtain Al<sub>2</sub>O<sub>3</sub> [6,10,12,13].

In this work, we study the use of thermally evaporated ultra-thin Al<sub>2</sub>O<sub>3</sub> layer in order to avoid the possible presence of hydrogen applied to the CZTS/CdS interface for passivation showing a clear effect on the V<sub>oc</sub> of the devices, as well as FF values which suggests a passivation effect on the CZTS surface.

## 2. EXPERIMENTAL DETAILS

CZTS thin films were grown onto Mo coated SLG glass by a sequential process. Stacked metallic films were deposited by DC magnetron sputtering (Alliance CT100) where Cu, Sn and Zn elemental targets were used. We obtained CZT precursor materials with slightly different copper content and Zn-rich as it has been reported elsewhere [14]. We investigated slightly Cu-poor, Cu-poor and very Cu-poor films (M1, M2 & M3, respectively) which cationic ratios are presented in Table II. The cationic ratios were determined by X-ray fluorescence (Fisherscope XVD). After deposition, the CZT precursors were simultaneously sulfurized inside of a graphite box containing sulfur and tin powders, using a tubular furnace and the following two-step annealing: 15 min at 200°C (1 mbar Ar flux) and 30 min at 550°C (1 bar total Ar pressure). Prior to the Al<sub>2</sub>O<sub>3</sub> deposition, the samples were etched using KCN solution (2% w/V, 2 min) [15]. A ~3nm Al<sub>2</sub>O<sub>3</sub> layer was deposited by thermal evaporation (Univex 250) at room temperature in some of the samples and, a 50 nm thick CdS buffer layer was then deposited by chemical bath deposition.

Finally, the devices were completed with i-ZnO (50 nm)/ITO (200 nm) layers deposited by DC magnetron sputtering (Alliance Ac450). In this way, two different architectures were studied: SLG/Mo/CZTS/CdS/i-ZnO/ITO and SLG/Mo/CZTS/Al<sub>2</sub>O<sub>3</sub>/CdS/i-ZnO/ITO. Individual 8.7 mm<sup>2</sup> solar cells were isolated using a manual microdiamond scribe and characterized by means J-V illuminated curves (AM 1.5) and external quantum efficiency (EQE).

The as-grown CZTS films were analyzed by Raman spectroscopy using a Horiba Jobin-Yvon FHR640 spectrometer coupled with a CCD camera and excited by a solid-state laser (532 nm) and He-Cd gas laser (325 nm). The measurements were performed in the backscattering configuration through a specific optical probe designed at IREC. X-Ray Diffraction patterns (XRD) were obtained by a diffractometer D8 Discover Bruker using CuK $\alpha_1$  ( $\lambda=1.5406\text{\AA}$ ) in 2 $\theta$  configuration. Transmittance and reflectance were obtained using an UV/Vis spectrometer Lambda 950, Perkin Elmer. Both top and cross section SEM images were taken using a Zeiss Series Auriga microscope using 5 kV as acceleration voltage.

J-V curves were measured under light conditions using a Sun 3000 class AAA Abet Technologies solar simulator (1 Sun illumination). The EQE measurements were obtained using a Bentham PVE3000 spectral response system calibrated with Si and Ge photodiodes.

TABLE II. COMPOSITION OF SAMPLES UNDER INVESTIGATION IN THIS WORK.

Sample	Zn/Sn	Cu/(Zn+Sn)	Al <sub>2</sub> O <sub>3</sub>
M1NA	1.21	0.74	No
M1WA	1.21	0.74	Yes
M2NA	1.06	0.72	No
M2WA	1.06	0.72	Yes
M3NA	1.15	0.70	No
M3WA	1.15	0.70	Yes

### 3. RESULTS AND DISCUSSION

#### 3.1 AS-GROWN SAMPLES.

Fig. 1 shows the typical Raman spectra obtained for the three type of samples utilized in this work for green (532 nm) and UV (325 nm) excitation wavelengths. In the spectra measured under 532 nm only the peaks related to CZTS compound were detected [15,16], while the low width of the main peak denotes the high crystalline quality of the sample. On the other hand, for the three cases, traces of ZnS were detected under 325 nm, independently from the type of sample. This can likely affect at some extent the optoelectronic properties of the solar cells, although it should not significantly influence the effect of the passivation layer. These Raman spectra show that the surface on all the samples is quite similar from the structural and secondary phases presence point of view.

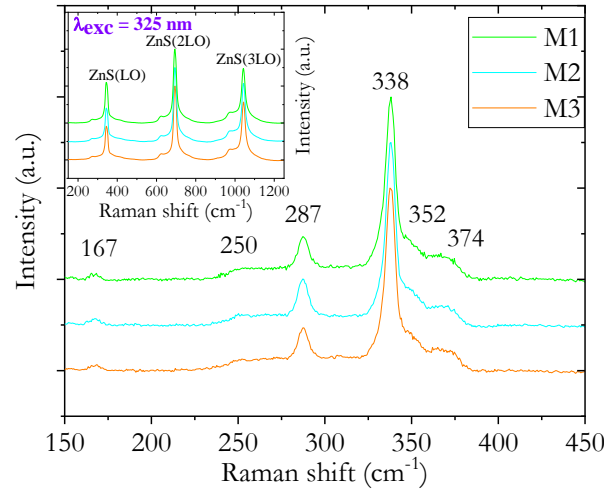


Fig. 1. Raman scattering spectra of the as-grown CZTS films with different Zn/Sn and Cu/(Zn+Sn) ratios, using 532 and 325 nm (inset) excitation wavelengths.

In order to further assess the crystalline properties of the layers, Fig. 2, shows the XRD patterns obtained in 2 $\theta$  configuration of samples M1, M2 and M3. In all the films the Cu<sub>2</sub>ZnSnS<sub>4</sub> kesterite phase (JCPDS Card No. 034-1246) is clearly present and is the dominating one, where the most intense peak is situated at 28.4° that is related to the (112) plane. Nevertheless, in the samples M2 (Cu/(Zn+Sn) = 0.72) and M3 (Cu/(Zn+Sn) = 0.70) two additional peaks were detected: at 30.26° and 46.11° that belong to the SnS<sub>2</sub> phase (JCPDS Card No. 022-0951). This phase is present when the Cu concentration is reduced and could be detrimental for solar cell devices performance [17-20]. From these measurements, it is hard to distinguish if SnS<sub>2</sub> is present at the interfaces or in the bulk of the absorber. This could affect, in consequence, the subsequent deposition of the Al<sub>2</sub>O<sub>3</sub> layer. On other hand, in order to obtain the crystallite size and uniform stress, we used the Williamson-Hall method [21]. First, we calculated the full width at half maximum ( $\beta_{hkl}$ ) for all the samples. Initially, the instrumental broadening ( $\beta_{hkl \text{ instrumental}}$ ) was corrected, corresponding to each diffraction peak of CZTS material, using the relation:

$$\beta_{hkl} = [(\beta_{hkl \text{ measured}})^2 - (\beta_{hkl \text{ instrumental}})^2]^{1/2} \quad (1)$$

Once corrected the  $\beta_{hkl}$ , we can calculate the crystallite size (D) and strain ( $\epsilon$ ) on the as-grown CZTS films, using the relation:

$$\beta_{hkl} \cos \theta = \frac{K\lambda}{D} + 4\epsilon \sin \theta \quad (2)$$

The relation (2) is the Williamson-Hall equation, where K is the shape factor,  $\lambda$  is the wavelength of the X-ray used, in our case  $\lambda=1.5406 \text{ \AA}$  and  $\theta$  is the Bragg angle. A plot is drawn with  $4\sin\theta$  along the x-axis and  $\beta_{hkl} \cos\theta$  along the y-axis. From the linear fit of the data, the crystallite size (D) was estimated from the y-intercept, and the strain ( $\epsilon$ ), from the slope of the fit [21]. The peaks used to obtain D and  $\epsilon$  were:  $2\theta=28.53^\circ$  (112),  $32.99^\circ$  (200),  $47.33^\circ$  (220) and  $56.18^\circ$  (312). In Fig. S1a, S1b and S1c are shown the Williamson-Hall plots from the samples M1, M2 and M3. In Table III are shown the values of  $\beta_{hkl}$  (from 112 plane on each sample), D and  $\epsilon$ .

TABLE III. STRUCTURAL PARAMETERS FROM AS-GROWN CZTS SAMPLES.

Sample	$\beta_{hkl}$ (°)	D (nm)	$\epsilon \times 10^{-4}$
M1	0.19	41	1.60
M2	0.11	83	2.88
M3	0.12	64	3.40

The values of  $\beta_{hkl}$  suggest that the M2 sample has slightly better crystalline quality than the sample M1 and M3. Sample M3 has more strain than the samples M1 and M2, this is related to crystal imperfections that could be related to poor Cu contents in the film.

The bandgap of the samples was estimated from transmittance and reflectance measurements. Fig. S2 shows the Tauc plots from which the bandgap energy ( $E_g$ ) of the three samples was obtained, using the follow relation [22]:

$$(\alpha h\nu)^n = A(h\nu - E_g) \quad (3)$$

where A is a constant and  $n=2$  or  $n=1/2$  for the direct and indirect bandgap transitions, respectively. The bandgap of the samples is M1=1.50 eV, M2=1.49 eV and, M3=1.47 eV. These values were calculated to discard possible changes in bandgap due to the  $Al_2O_3$  deposition process.

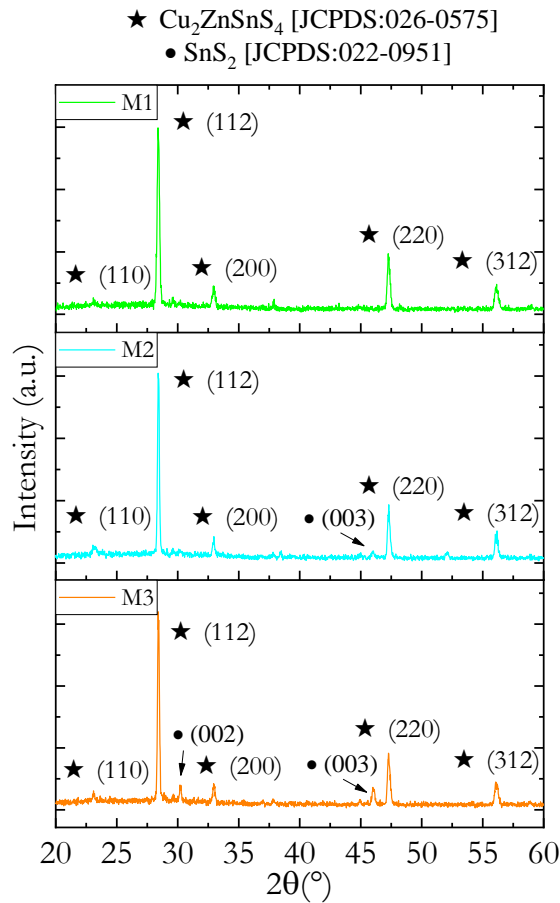


Fig. 2. X-ray Diffraction of samples M1, M2 and, M3.

In Fig. 3 we present the top-view images from the as-grown films (M1, M2 and, M3). All the samples exhibit a similar morphology, although the M1 layer exhibits smaller grain size at the surface that could be related to the presence of binary secondary phases such as ZnS or Cu<sub>2</sub>S<sub>x</sub> phases [23-24]. The top-view of the M1 sample is shown in Fig. 3 a), where the grain size is estimated to be between 0.5 μm and 1 μm.

In addition, the top-view of the M2 is shown in Fig. 3 b), where the film exhibits grain sizes between 0.4 μm and 2 μm and, with some surface voids are clearly seen. Fig 3 c) reveals a larger amount of surface voids and grains with similar sizes as M2 (0.6 μm to 2.2) μm. In principle, the surface voids could severely affect the properties of the solar cells by decreasing the shunt resistance and deteriorating the FF, as it is observed in the devices behavior reported in Fig. 4a). In this case, the presence of Al<sub>2</sub>O<sub>3</sub> can act as insulating layer preventing the shunt-paths, and then contributing to the observed FF improvement.

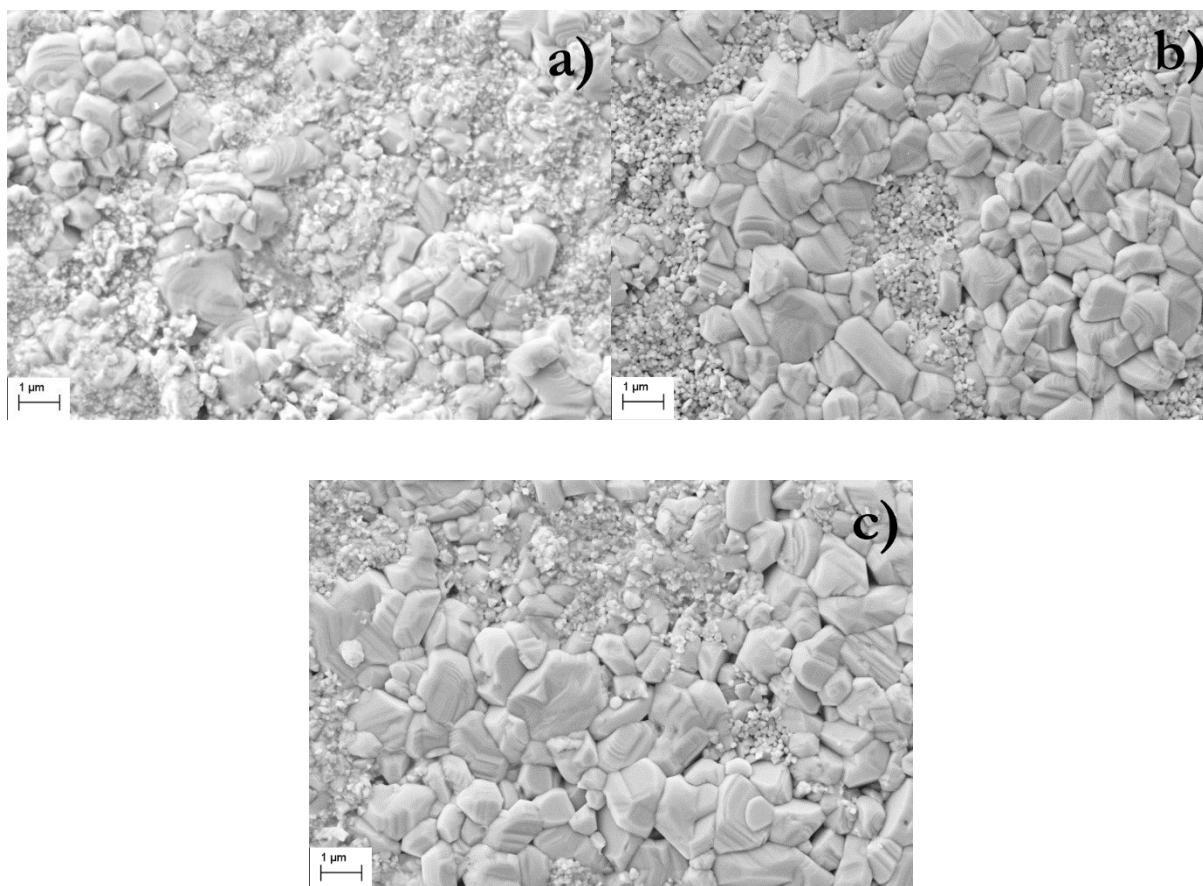


Fig. 3. Top-view SEM images from the as-grown films. a) M1, b) M2 and, c) M3.

### 3.2 CZTS SOLAR CELLS WITH AND WITHOUT Al<sub>2</sub>O<sub>3</sub>.

After the analysis of the as-grown films, the analysis of the solar cell devices fabricated with them is presented. The denotation of the solar cells is: M1NA, M2NA and, M3NA are the cells without Al<sub>2</sub>O<sub>3</sub> intermediate nanolayer and finally, the cells M1WA, M2WA and, M3WA are the cells with Al<sub>2</sub>O<sub>3</sub> intermediate nanolayer. The J-V curves illuminated characteristics for the three type of the samples under investigation (with and without Al<sub>2</sub>O<sub>3</sub> intermediate nanolayer) are shown in Fig. 4. In Fig. 4 a), b) and, c) are showed samples M1NA & M1WA, M2NA & M2WA, M3NA & M3WA, respectively. In Fig 4a) sample M1WA showed an increment in V<sub>oc</sub> of +23 mV, but a decrement of ~1.4 mA/cm<sup>2</sup>. In Fig 4b) sample M2WA showed an increment in V<sub>oc</sub> of +26

mV and the best efficiency of all the samples, showing an efficiency ( $\eta$ ) of 6.1%. In Fig. 4c) the sample M3WA showed an increment in  $V_{oc}$  of +35 mV and a decrement of 0.4 mA/cm<sup>2</sup> in  $J_{sc}$ .

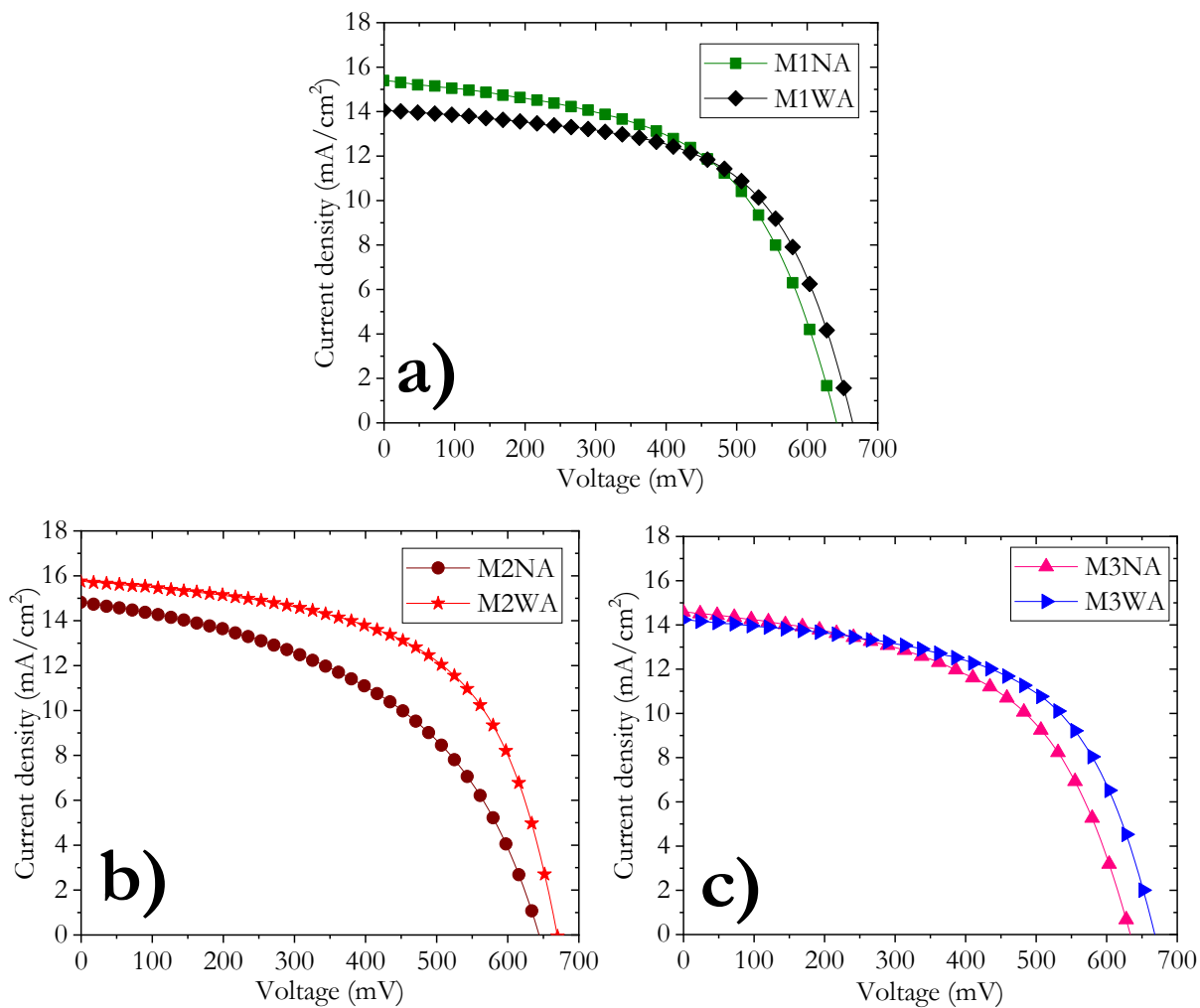


Fig. 4. J-V characteristics of a) M1NA & M1WA, b) M2NA & M2WA, c) M3NA & M3WA.

TABLE IV. ELECTRICAL PARAMETERS OF CZTS SOLAR CELLS WITHOUT AND WITH Al<sub>2</sub>O<sub>3</sub>.

Sample	J <sub>sc</sub> (mA/cm <sup>2</sup> )	V <sub>oc</sub> (mV)	FF (%)	$\eta$ (%)	G <sub>sh</sub> (mS/cm <sup>2</sup> )	R <sub>s</sub> ( $\Omega$ cm <sup>2</sup> )	A	J <sub>0</sub> (mA/cm <sup>2</sup> )
M1NA	15.4	641	55.4	5.4	0.08	4.2	1.82	3.46x10 <sup>-6</sup>
M2NA	14.8	643	47.6	4.5	0.15	4.1	1.98	1.61x10 <sup>-3</sup>
M3NA	14.6	633	53.2	4.9	0.13	20.5	2.10	3.21x10 <sup>-5</sup>
M1WA	14	664	59.2	5.5	0.08	7.3	1.81	9.47x10 <sup>-7</sup>
M2WA	15.7	669	58	6.1	0.04	4.2	1.68	1.21x10 <sup>-5</sup>
M3WA	14.2	668	57.5	5.5	4.33	5.9	2.00	3.06x10 <sup>-3</sup>

In Table IV are shown the electrical parameters of the solar cells without and with Al<sub>2</sub>O<sub>3</sub>. The difference in  $\eta$  between the samples M1NA, M2NA and, M3NA could be related to the presence of secondary phases in M2NA and M3NA (such as SnS<sub>2</sub> as was shown by XRD) and its n-type nature that could affect directly the performance of the solar cells [19, 25, 26].

Independently from the compositional regime with which we are working, the Al<sub>2</sub>O<sub>3</sub> passivation layer seems to help to increase the  $V_{oc}$  values in all the samples. In this case, the improvement is not related to the presence of species containing hydrogen but rather to Al<sub>2</sub>O<sub>3</sub> itself.

To obtain the information of the loss mechanisms present in the fabricated CZTS solar cells, the diode parameters were calculated, such as, shunt conductance ( $G_{sh}$ ) (Fig. S3), series resistance ( $R_s$ ) (Fig. S4), ideality factor ( $A$ ) (Fig. S4) and the saturation current density ( $J_0$ ) (Fig. S5). The J-V dark curves were used to obtain these parameters, using Sites' method [27, 28]. The  $G_{sh}$  of the samples is in accordance with the common value reported for kesterite solar cells [3,6]. The series resistance agrees with the values obtained in CZTS solar cells, except for the M3NA samples with a value of 20.5  $\Omega\text{cm}^2$  [6]. The high value in  $R_s$  could be attributed to the growing of MoS<sub>2</sub> in the Mo/CZTS interface and could affect directly the fill factor of the solar cell [29]. The  $J_0$  values of the samples without Al<sub>2</sub>O<sub>3</sub> are larger than those of the samples with Al<sub>2</sub>O<sub>3</sub>, only in the case of samples M1 and M2. The decrease of the  $J_0$  values with Al<sub>2</sub>O<sub>3</sub> could be due to a reduced recombination. To understand the effect of Al<sub>2</sub>O<sub>3</sub> it is important to know the two kinds of passivation mechanisms that the Al<sub>2</sub>O<sub>3</sub> could perform. As Dingemans *et al.* [30] reported, the passivation of Al<sub>2</sub>O<sub>3</sub> can generate two types of reduction of recombination: chemical passivation and field-effect passivation [12]. The chemical passivation consists in a reduction of surface recombination ( $U_s$ ), which arises from the variations in structure, due to dangling bonds or deep defects that are distributed throughout the bandgap. These dangling bonds or deep defects are part of the interface defect density ( $N_{it}$ ) [30]. On the other hand, the field effect passivation consists in reducing the  $U_s$  diminishing the electron or hole density at the surface or interface (of the solar cell) by an electric field due to a Coulomb repulsion [12, 30, 31]. In the same way, an important factor of the passivation with Al<sub>2</sub>O<sub>3</sub> is the thickness of the film. It was demonstrated that a high level of surface passivation could be maintained down to approximately 10 nm [30, 32]. The cause of the deterioration (due to a possible annealing during the solar cell fabrication) is a decrease in the chemical passivation. It has been reported that the field-effect passivation is constant while decreasing the film thickness to 2 nm [30, 33]. With this information we can clarify that the dominant passivation effect is the chemical passivation effect, due to the quantity of deep defects or dangling bonds that could have at the the interface related to the  $V_{oc}$  increment, that showed the solar cells and having a lower  $J_0$  value. Additionally, the ideality factor is an important parameter that shows the dominant charge transport mechanism. If the ideality factor becomes 1, the diffusion current is more than recombination current. Conversely, if the recombination current is more than diffusion current, the ideality factor becomes 2. If the ideality factor is bigger than 2, the current transport in the grain boundary region of the material is controlled by a recombination at a high density of defect states [34]. In our case, only the sample M2 showed a significant reduction in  $A$  from 1.98 (M2NA) to 1.68 (M2WA). Furthermore, it showed the effect of the Al<sub>2</sub>O<sub>3</sub> deposited by thermal evaporation.

Additionally, the external quantum efficiency (EQE) was measured in all samples (Fig. 5). All the samples without Al<sub>2</sub>O<sub>3</sub> showed an EQE with a maximum near 70%. On the other hand, the samples with Al<sub>2</sub>O<sub>3</sub> showed an improvement in response with a maximum near 72%, in all the cases. It is observed that the optical response in the short wavelength region is very slightly improved with the Al<sub>2</sub>O<sub>3</sub> passivation layer. It can be noted that in the 400-600 nm region the carrier collection is improved for the three compositions under investigation, suggesting a general improvement of the CZTS/CdS near the interface region that we tentatively assign to the passivation effect due to the introduction of the Al<sub>2</sub>O<sub>3</sub> nanolayer. From the EQE we can obtain the bandgap using the inflection of the  $dEQE/d\lambda$  curves [35]. In Table V is shown a summary of the  $E_g$  values obtained from Tauc plot (as-

grown samples) and  $dEQE/d\lambda$  curves (with the solar cell fabricated). Moreover, we include the Urbach energy ( $E_U$ ) to characterize the tail of the bandgap. The  $E_U$  is from the inverse of the slope of the linear region below the bandgap [36,37]. The Urbach Energy curves are shown in Fig. S6 and Fig. S7.

TABLE V. SUMMARY OF THE  $E_G$  VALUES FROM THE AS-GROWN SAMPLES AND THE SOLAR CELLS.

<b>Sample.</b>	<b>Tauc plot (eV)</b>	<b>dEQE/d<math>\lambda</math> (eV)</b>	<b>Urbach energy (meV)</b>
<b>M1NA</b>	1.50	1.50	73
<b>M2NA</b>	1.49	1.53	65
<b>M3NA</b>	1.47	1.52	71
<b>M1WA</b>	1.50	1.51	74
<b>M2WA</b>	1.49	1.51	68
<b>M3WA</b>	1.47	1.51	71

From the Table V is implicit that there is no significant difference among the bandgap values. On the other hand, from the Urbach Energy, this is to characterize the tail of the bandgap. We can see that there is not a big difference without and with  $Al_2O_3$ . This means that the  $Al_2O_3$  film deposition did not change the antisite defects in the bulk material. The effect of the  $Al_2O_3$  was only on the surface and with that it was enough to improve the  $V_{oc}$  [38].

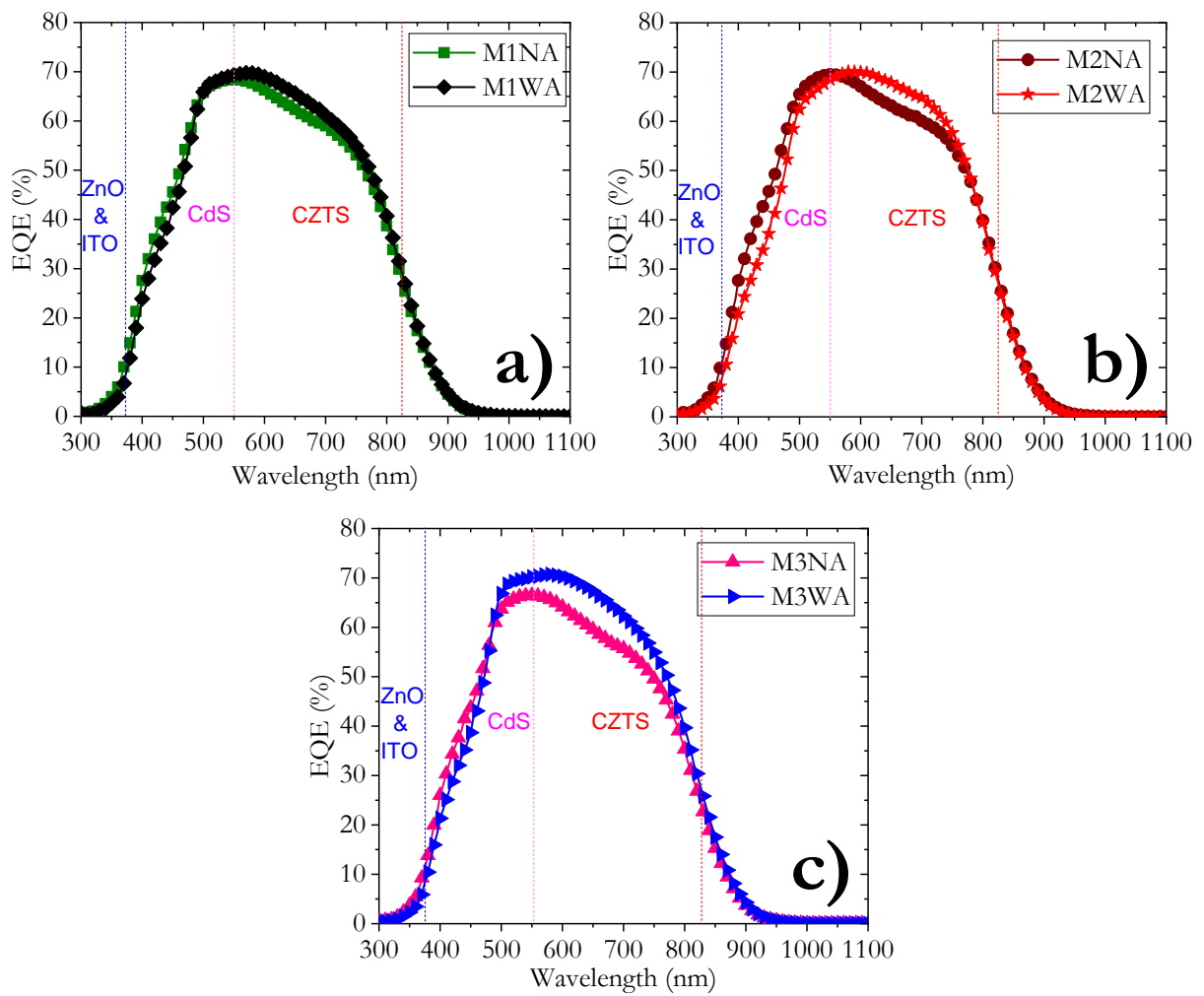


Fig. 5. EQE of CZTS solar cells a) M1NA & M1WA, b) M2NA & M2WA, c) M3NA & M3WA.

In Fig. 6. it is shown the cross-section image from the best performance sample (M2WA). At the back contact of the solar cells, some voids between the molybdenum layer and the CZTS absorber are observed, that could be due to the formation of the  $\text{MoS}_2$  layer and the concomitant reported instability of kesterite when it is in direct contact with Mo [39-40]. Of course, the interface between the  $\text{Al}_2\text{O}_3$  and CdS nanolayers is not clear due to the reduced thickness of these layers, mainly the  $\text{Al}_2\text{O}_3$ . The thicknesses of all the layers were determined as follows: Mo (~ 650 nm),  $\text{MoS}_2$  (~90 nm), CZTS (~1.4  $\mu\text{m}$ ),  $\text{Al}_2\text{O}_3$ +CdS (~50 nm) and (ZnO+ITO) (~200 nm), among the expected values for this type of technology.

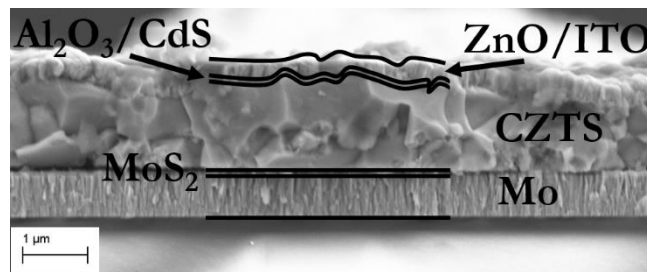


Fig. 6. Cross-section SEM of the sample M2WA.

Finally, in order to get a better understanding of the application of the  $\text{Al}_2\text{O}_3$  on the interface between CZTS/CdS, in Fig. 7a) depicts a simplified band schema of the CZTS/CdS/ZnO/FTO structure and Fig. 7b) depicts a simplified band schema of the CZTS/ $\text{Al}_2\text{O}_3$ /CdS/ZnO/FTO. The conduction band offset (CBO) of the CZTS/CdS from the Fig. 7a) and CZTS/ $\text{Al}_2\text{O}_3$ ,  $\text{Al}_2\text{O}_3$ /CdS interfaces were estimated using the values reported in the literature, as well as the electron affinities of each compound [41-47]. The bandgap diagrams were estimated using SCAPS software. It is known that a spike-like CBO in CZTS/CdS heterojunction is one of the major drawbacks for the correct performance of the CZTS solar cells causing losses in the  $V_{oc}$  [48, 49]. The CBO of the CZTS/CdS junction in Fig. 7a) is  $\sim 0.35$  eV and  $\sim 0.25$  eV, respectively. In the same way, the valence-band offsets (VBO) of the CZTS/CdS and CdS/ZnO junctions are  $\sim 1$  eV and  $\sim 1.2$  eV, respectively.

As is shown in Fig. 7b), with the addition of the  $\text{Al}_2\text{O}_3$  nanolayer into the CZTS/CdS heterojunction, a very large spike-like CBO is created at the CZTS/ $\text{Al}_2\text{O}_3$  and  $\text{Al}_2\text{O}_3$ /CdS interfaces. The values are about 1.5 eV and 1.2 eV, respectively; which can be extremely large for this type of devices. Nevertheless, considering the very thin nature of the  $\text{Al}_2\text{O}_3$  layer (less than 3 nm), electrons can relatively easily tunnel this barrier for being collected in the electron selective contact of the solar cell. By the same way, these electrons can avoid the interface recombination, due to the chemical passivation created by the  $\text{Al}_2\text{O}_3$ . In the case of CZTS/ $\text{Al}_2\text{O}_3$  junction, the VBO is  $\sim 4.1$  eV, and for  $\text{Al}_2\text{O}_3$ /CdS junction the VBO is  $\sim 3.1$  eV. The VBO of CZTS/ $\text{Al}_2\text{O}_3$ , may contribute to have a better selectivity for electrons in the heterojunction. In this sense, the resulting structure can be in principle assimilated as a p-i-n type device. In fact, it is relatively important to keep the  $\text{Al}_2\text{O}_3$  layer as thin as possible to allow the formation of the space charge region, as showed by H. Sun *et. al* [9] but guaranteeing the passivation of the defects in CZTS/CdS interface [50].

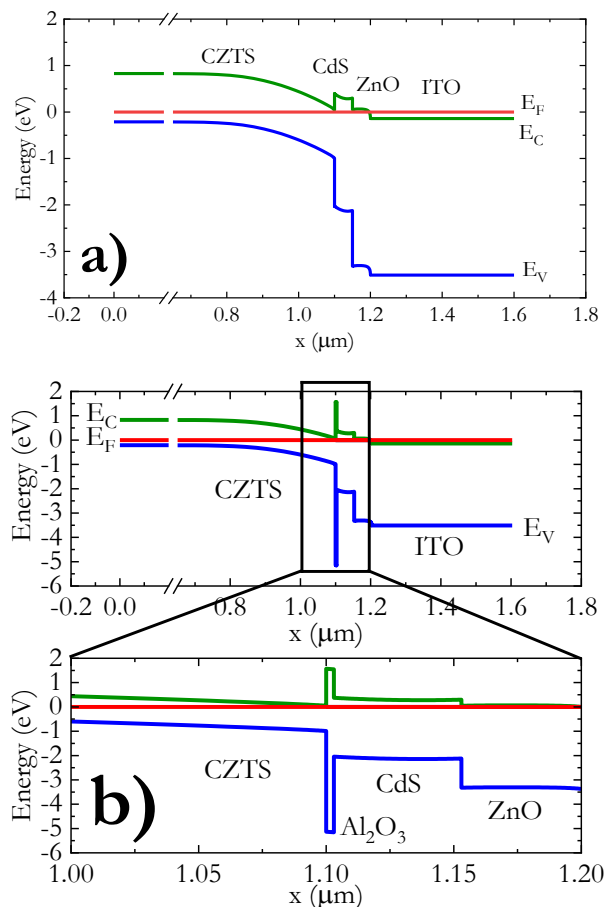


Fig. 7. Simplified band schemas of the a) CZTS/CdS/ZnO/FTO and, b) CZTS/ $\text{Al}_2\text{O}_3$ /CdS/ZnO/FTO structures.

#### 4. CONCLUSIONS

We proved that thermally evaporated Al<sub>2</sub>O<sub>3</sub> ultra-thin layers (down to 3 nm) can be used as passivation layer for CZTS/CdS heterojunctions, with a demonstrated enhancement on the V<sub>oc</sub> and FF of the solar cell devices. In particular, the use of evaporated layers from an Al<sub>2</sub>O<sub>3</sub> source demonstrates that hydrogen related species are not indispensable for the passivation, and that the pure oxide is an efficient passivation agent. We suggest the chemical passivation effect as dominant passivation mechanism. Additional evidences of the passivation effects are obtained with the observed photo-response improved in the light spectrum region between 400 and 550 nm, suggesting a better collection of the light absorbed located in p-n junction region. In summary, the evaporated Al<sub>2</sub>O<sub>3</sub> nanolayers not only enhance the properties of the CZTS based solar cell, but also passivate the defects on the surface whereby it results in a very simple methodology to be applied for improving the kesterite technology.

#### 5. ACKNOWLEDGEMENTS

This research was supported by the H2020 Programme under the project INFINITE-CELL (H2020-MSCA-RISE-2017-777968), by the Spanish Ministry of Science, Innovation and Universities under the IGNITE project (ENE2017-87671-C3-1-R), and by the European Regional Development Funds (ERDF, FEDER Programa Competitivitat de Catalunya 2007-2013). Authors from IREC and the University of Barcelona belong to the SEMS (Solar Energy Materials and Systems) Consolidated Research Group of the “Generalitat de Catalunya” (Ref. 2017 SGR 862). M.P. thanks the Government of Spain for the Ramon y Cajal Fellowship (RYC-2017-23758). This research was also supported by Consejo Nacional de Ciencia y Tecnología (CONACYT) with the scholarship No. 433146 and with the project CB-CONACYT-255062. Finally, this research was also supported by Programa de Fortalecimiento de la Calidad Educativa (PFCE 2019) and by Project VIEP 2019. Authors also want to thank to Dra. Primavera López Salazar (CIDS-ICUAP) for helping with XRD measurements.

#### 6. REFERENCES

- [1] S. Giraldo, Z. Jehl, M. Placidi, V. Izquierdo-Roca, A. Pérez-Rodríguez, E. Saucedo. “Progress and Perspectives of Thin Film Kesterite Photovoltaic Technology: A Critical Review”. *Adv. Mater.* 2019, 31, 1806692. DOI: 10.1002/adma.201806692.
- [2] V. Fthenakis. “Sustainability of photovoltaics: The case for thin-film solar cells”. *Renew. Sust. Energ. Rev.* 13, 2746 (2009).
- [3] W. Wang, Mark T. Winkler, O. Gunawan, T. Gokmen, T.K. Todorov, Y. Zhu, D.B. Mitzi. “Device characteristics of CZTSSe thin-film solar cells with 12.6% efficiency”. *Adv. Energy Mater.* Vol. 4, 1301465, 2014. DOI:10.1002/aenm.201301465.
- [4] P. Jackson, R. Wuerz, D. Hariskos, E. Lotter, W. White, M. Powalla “Effects of heavy alkali elements in Cu(In,Ga)Se<sub>2</sub> solar cells with efficiencies up to 22.6%” *Physica Status Solidi (RRL)*. Vol. 10, 583-586, 2018. DOI: 10.1002/pssr.201600199.
- [5] M. Courel, J.A. Andrade-Arvizu, O. Vigil-Galán. “Loss mechanisms influence on Cu<sub>2</sub>ZnSnS<sub>4</sub>/CdS-based thin film solar cell performance” *Solid-State Electronics*. Vol. 111, 243-250, 2015. DOI: 10.1016/j.sse.2015.05.038.
- [6] C. Yan J. Huang, K. Sun, S. Johnston, Y. Zhang, H. Sun, A. Pu, M. He, F. Liu, K. Eder, L. Yang, J.M. Cairney, N.J. Ekins-Daukes, Z. Hameiri, J.A. Stride, S. Chen, M.A. Green, X. Hao. “Cu<sub>2</sub>ZnSnS<sub>4</sub> solar cells with over 10% power conversion efficiency enabled by heterojunction heat treatment”. *Nature energy*. 3, 764-772 (2018). DOI: 10.1038/s41560-018-0206-0.
- [7] F. Zhou, F. Zeng, X. Liu, F. Liu, N. Song, C. Yan, A. Pu, J. Park, K. Sun, X. Hao. “Improvement of J<sub>sc</sub> in a Cu<sub>2</sub>ZnSnS<sub>4</sub> solar cell by using a thin carbon intermediate layer at the Cu<sub>2</sub>ZnSnS<sub>4</sub>/Mo interface”. *Appl. Mater. Interfaces*. Vol. 7, 22868-22873, 2015. DOI: 10.1021/acsami.5b05652.

- [8] H. Cui, X. Liu, F. Liu, X. Hao, N. Song, C. Yan. "Boosting  $\text{Cu}_2\text{ZnSnS}_4$  solar cells efficiency by a thin Ag intermediate layer between absorber and back contact". *Appl. Phys. Letters*. Vol. 104, 041115, 2014. DOI: 10.1063/1.4863951.
- [9] H. Sun, K. Sun, J. Huang, C. Yan, F. Liu, J. Park, A. Pu, J.A. Stride, M.A. Green and X. Hao. "Efficiency enhancement of kesterite  $\text{Cu}_2\text{ZnSnS}_4$  solar cells via solution-processed ultrathin tin oxide intermediate layer at absorber/buffer interface" *ACS Appl. Energy Mater.*, vol. 1, 154-160, 2018. DOI:10.1021/acsaem.7b00044.
- [10] J. Park, J. Huang, J. Yun, F. Liu, Z. Ouyang, H. Sun, C. Yan, K. Sun, K. Kim, J. Seidel, S. Chen, M.A. Green, X. Hao. "The role of hydrogen from ALD- $\text{Al}_2\text{O}_3$  in kesterite  $\text{Cu}_2\text{ZnSnS}_4$  solar cells: grain surface passivation." *Adv. Energy Mater.* 1701940, 1-7, 2018. DOI: 10.1002/aenm.201701940.
- [11] H. Xie, Y. Sánchez, P. Tang, M. Espíndola-Rodríguez, M. Guc, L. Calvo-Barrio, S. López-Marino, Y. Liu, J. R. Morante, A. Cabot, V. Izquierdo-Roca, J. Arbiol, A. Pérez-Rodríguez, E. Saucedo. "Enhanced hetero-junction quality and performance of kesterite solar cells by Aluminum Hydroxide nanolayers and efficiency limitation revealed by Atomic-resolution scanning transmission electron microscopy". *Sol. RRL* 2019, 3, 1800279. DOI: 10.1002/solr.201800279.
- [12] M. E. Erkan, V. Chawla, M. A. Scarpulla. "Reduced defect density at the CZTSSe/CdS interface by atomic layer deposition of  $\text{Al}_2\text{O}_3$ ". *J. Appl. Phys.* 2016, 119, 194504. DOI:10.1063/1.4948947.
- [13] Y. S. Lee, T. Gershon, T. K. Todorov, W. Wang, M. T. Winkler, M. Hopstaken, O. Gunawan, J. Kim. "Atomic Layer Deposited Aluminum Oxide for Interface Passivation of  $\text{Cu}_2\text{ZnSn}(\text{S},\text{Se})_4$  Thin-Film Solar Cells". *Adv. Energy Mater.* 2016, 6, 1600198. DOI: 10.1002/aenm.201600198.
- [14] S. van Duren, D. Sylla, A. Fairbrother, Y. Sánchez, S. López-Marino, J. A. Márquez Prieto, V. Izquierdo-Roca, E. Saucedo, T. Unold. "Pre-annealing of metal stack precursors and its beneficial effect on kesterite absorber properties and device performance". *Sol. Energy Mater. Sol. Cells* 2018, 185, 226-232. DOI: 10.1016/j.solmat.2018.04.022
- [15] A. Fairbrother, E. García-Hemme, V. Izquierdo-Roca, X. Fontané, F.A. Pulgarín-Agudelo, O. Vigil-Galán, A. Pérez-Rodríguez, E. Saucedo. "Development of a selective chemical etch to improve the conversion efficiency of Zn-rich  $\text{Cu}_2\text{ZnSnS}_4$  solar cells". *J. Am. Chem. Soc.* Vol. 134, 8018-8021, 2012. DOI: 10.1021/ja301373e
- [16] M. Guc, S. Levchenko, I. V. Bodnar, V. Izquierdo-Roca, X. Fontane, L. V. Volkova, E. Arushanov, A. Pérez-Rodríguez. "Polarized Raman scattering study of kesterite type  $\text{Cu}_2\text{ZnSnS}_4$  single crystals". *Sci. Rep.* Vol. 6, 19414, 2016. DOI:10.1038/srep19414.
- [17] F. Oliva, L. Arqués, L. Acebo, M. Guc, Y. Sánchez, X. Alcobé, A. Pérez-Rodríguez, E. Saucedo, V. Izquierdo-Roca. "Characterization of  $\text{Cu}_2\text{SnS}_3$  polymorphism and its impact on optoelectronic properties". *J. Mater. Chem. A*, 2017, 5, 23863. DOI: 10.1039/c7ta08705e.
- [18] M. Kumar, A. Dubey, N. Adhikari, S. Venkatesan and Q. Qiao, "Strategic review of secondary phases, defects and defect-complexes in kesterite CZTS-Se solar cells", *Energy Environ. Sci.*, 2015, 8, 3134–3159. DOI: 10.1039/c5ee02153.
- [19] W. Wang, G. Chen, H. Cai, B. Chen, L. Yao, M. Yang, S. Chen and Z. Huang. "The effects of  $\text{SnS}_2$  secondary phases on  $\text{Cu}_2\text{ZnSnS}_4$  solar cells: a promising mechanical exfoliation method for its removal" *J. Mater. Chem. A.*, 2018, 6, 2995. DOI: 10.1039/c7ta08242h
- [20] S. C. Ray, M. K. Karanjai, D. DasGupta. "Structure and photoconductive properties of dip-deposited SnS and  $\text{SnS}_2$  thin films and their conversion to tin dioxide by annealing in air" *Thin Solid Films*, 350 (1999) 72-78. DOI: 10.1016/S0040-6090(99)00276-X.
- [21] V.D. Mote, Y. Purushotham, B.N. Dole. "Williamson-Hall analysis in estimation of lattice strain in nanometer-sized ZnO particles". *J. Theor. Appl. Phys.* (2012) 6: 6. <https://doi.org/10.1186/2251-7235-6-6>.
- [22] J. I. Pankove. *Optical Processes in Semiconductors* (New York: Dover) p.36.
- [23] W. Li, J. Chen, C. Yan, X. Hao. "The effect of ZnS segregation on Zn-rich CZTS thin film solar cells". *J. Alloy. Compd.* 632 (2015) 178-184. DOI: 10.1016/j.jallcom.2015.01.205.
- [24] O. Awadallah, Z. Cheng. "In Situ Raman characterization of  $\text{Cu}_2\text{ZnSnS}_4$  solar absorber material". *2015 IEEE 42nd Photovoltaic Specialist Conference (PVSC)*. DOI:10.1109/PVSC.2015.7355595.
- [25] J. H. Kim, S. J. Yun, H. S. Lee, J. Zhao, H. Bouzid and Y. H. Lee. "Plasma-induced phase transformation of  $\text{SnS}_2$  to SnS". *Nature. Scientific Reports*. 8: 10284 (2018). DOI:10.1038/s41598-018-28323-y.

- [26] J.-H. Ahn, M.-J. Lee, H. Heo, J. H. Sung, K. Kim, H. Hwang and M.-H. Jo. "Deterministic two-dimensional polymorphism growth of hexagonal n-type SnS<sub>2</sub> and orthorhombic p-type SnS crystals". *Nano Lett.*, 2015, 15 (6), pp 3703–3708. DOI: 10.1021/acs.nanolett.5b00079.
- [27] J. R. Sites, P. H. Mauk. "Diode quality factor determination for thin-film solar cells". *Solar cells*, 27 (1989) 411-417. [https://doi.org/10.1016/0379-6787\(89\)90050-1](https://doi.org/10.1016/0379-6787(89)90050-1)
- [28] S. S. Hegedus, W. N. Shafarman. "Thin-film solar cells: device measurements and analysis". *Prog. Photovolt: Res. Appl.* 2004; 12: 155-176. DOI: 10.1002/pip.518.
- [29] U. V. Ghorpade, M. P. Suryawanshi, S. W. Shin, I. Kim, S. K. Ahn, J. H. Yun, C. Jeong, S. S. Kolekar, J. H. Kim. "Colloidal wurtzite Cu<sub>2</sub>SnS<sub>3</sub> (CTS) nanocrystals and their applications in solar cells". *Chem. Mater.* 2016, 28, 3308-3317. DOI: 10.1021/acs.chemmater.6b00176.
- [30] G. Dingemans, W. M. M. Kessels. "Status and prospects of Al<sub>2</sub>O<sub>3</sub>-based surface passivation schemes for silicon solar cells". *J. Vac. Sci. Technol. A*, 30 040802 (2012). DOI: <http://dx.doi.org/10.1116/1.4728205>.
- [31] Armin G. Aberle, Stefan Glunz, Wilhelm Warta. "Field effect passivation of high efficiency silicon solar cells". *Sol. Energ. Mat. Sol. C* 29 (1993) 175-182. DOI: [https://doi.org/10.1016/0927-0248\(93\)90075-E](https://doi.org/10.1016/0927-0248(93)90075-E)
- [32] P. Saint-Cast, Y.-H. Heo, E. Billot, P. Olwal, M. Hofmann, J. Rentsch, S. W. Glunz, R. Preu. "Variation of the layer thickness to study the electrical property of PECVD Al<sub>2</sub>O<sub>3</sub>/c-Si interface". *Energy Procedia* 8 (2011) 642. DOI: <https://doi.org/10.1016/j.egypro.2011.06.195>
- [33] N.M. Terlinden, G. Dingemans, M.C. M. van de Sanden, and, W. M. M. Kessels. "Role of field-effect on c-Si surface passivation by ultrathin (2-20 nm) atomic layer deposited Al<sub>2</sub>O<sub>3</sub>". *Appl. Phys. Lett.* 96, 112101 (2010). DOI: <https://doi.org/10.1063/1.3334729>
- [34] S. S. Mali, P. S. Shinde, C. A. Betty, P. N. Bhosale, Y. W. Oh, P. S. Patil. "Synthesis and characterization of Cu<sub>2</sub>ZnSnS<sub>4</sub> thin films by SILAR method". *J. Phys. Chem. Solids*. 73 (2012) 735-740. DOI: <https://doi.org/10.1016/j.jpcs.2012.01.008>
- [35] T. Gokmen, O. Gunawan, T. K. Todorov, D. Mitzi. "Band tailing and efficiency limitation in kesterite solar cells". *Appl. Phys. Lett.* 103, 103506 (2013). DOI: <https://doi.org/10.1063/1.4820250>
- [36] A. Guchhait, Z. Su, Y. F. Tay, S. Shukla, W. Li, S. W. Leow, J. M. R. Tan, S. Lie, O. Gunawan, L. H. Wong. "Enhancement of Open-circuit voltage of solution-processed Cu<sub>2</sub>ZnSnS<sub>4</sub> solar cells with 7.2% efficiency by incorporation of silver". *ACS Energy Lett.* 2016, 1, 1256-1261. DOI: 10.1021/acsenerylett.6b00509.
- [37] S. López-Marino, Y. Sánchez, M. Placidi, A. Fairbrother, M. Espindola-Rodríguez, X. Fontané, V. Izquierdo-Roca, J. López-García, L. Calvo-Barrio, A. Pérez-Rodríguez, E. Saucedo. "ZnSe etching of Zn-rich Cu<sub>2</sub>ZnSnSe<sub>4</sub>: An oxidation route for improved solar-cell efficiency". *Chem. Eur. J.* 2013, 19, 14814-14822. DOI: 10.1002/chem.201302589.
- [38] H. Xie, S. López-Marino, T. Olar, Y. Sánchez, M. Neuschitzer, F. Oliva, S. Giraldo, V. Izquierdo-Roca, I. Lauer mann, A. Pérez-Rodríguez, E. Saucedo. "Impact of Na dynamics at the Cu<sub>2</sub>ZnSn(S,Se)<sub>4</sub>/CdS Interface during post low temperature treatment of absorbers. *ACS Appl. Mater. Interfaces*. 2016, 8, 5017-5024. DOI: 10.1039/acsami.5b12243.
- [39] S. López-Marino, M. Placidi, A. Pérez-Tomás, J. Llobet, V. Izquierdo-Roca, X. Fontané, A. Fairbrother, M. Espindola-Rodríguez, D. Sylla, A. Pérez-Rodríguez, E. Saucedo. "Inhibiting the absorber/Mo-back contact decomposition reaction in Cu<sub>2</sub>ZnSnSe<sub>4</sub> solar cells: the role of a ZnO intermediate nanolayer". *J. Mater. Chem. A*. 2013, 1, 8338. DOI: 10.1039/c3ta11419h.
- [40] J. J. Scragg, J. T. Wätjen, M. Edoff, T. Ericson, T. Kubart, C. Platzer-Björkman. "A detrimental reaction at the molybdenum back contact in Cu<sub>2</sub>ZnSn(S,Se)<sub>4</sub> thin-film solar cells". *J. Am. Chem. Soc.* 2012, 134(47), 19330-19333. DOI:10.1021/ja308862n.
- [41] M. L. Huang, Y. C. Chang, C. H. Chang, T. D. Lin, J. Kwo, T. B. Wu, M. Hong. "Energy-band parameters of atomic-layer-deposition Al<sub>2</sub>O<sub>3</sub>/InGaAs heterostructure. *Appl. Phys. Lett.* 89, 012903 (2006). DOI: <https://doi.org/10.1063/1.2218826>
- [42] M. Bär, B.-A. Schubert, B. Marsen, R. G. Wilks, S. Pookpanratana, M. Blum, S. Krause, T. Unold, W. Yang, L. Weinhardt, C. Heske, and H. -W. Schock. "Cliff-like conduction band offset and KCN-induced recombination barrier enhancement at the CdS/Cu<sub>2</sub>ZnSnS<sub>4</sub> thin-film solar cell heterojunction". *Appl. Phys. Lett.* 99, 222105 (2011). DOI:10.1063/1.3663327.
- [43] A. Crovetto, O. Hansen. "What is the band alignment of Cu<sub>2</sub>ZnSn(S,Se)<sub>4</sub> solar cells?". *Sol. Energy Mater. Sol. Cells*. 169 (2017) 177-194. DOI: 10.1016/j.solmat.2017.05.008.

- [44] A. Santoni, F. Biccari, C. Malerba, M. Valentini, R. Chierchia and A. Mittiga. "Valence band offset at the CdS/Cu<sub>2</sub>ZnSnS<sub>4</sub> interface probed by X-ray photoelectron spectroscopy. *J. Phys. D: Appl. Phys.* 46 (2013) 175101. DOI: 10.1088/0022-3727/46/17/175101.
- [45] N. B. Kindig and W. E. Spicer. "Band Structure of Cadmium Sulfide-Photoemission studies". *Phys. Rev.* 2A, 138, A561 (1965). DOI: 10.1103/PhysRev.138.A561.
- [46] A. Klein. "Energy band alignment in chalcogenide thin film solar cells from photoelectron spectroscopy". *J. Phys. Condens. Matter.* 27 (2015) 134201. DOI: 10.1088/0953-8984/27/13/134201.
- [47] J. Robertson and B. Falabretti. "Band offsets of high K gate oxide on III-V semiconductors". *J. Appl. Phys.* 100, 014111 (2006). DOI: 10.1063/1.2213170.
- [48] A. Crovetto, M. Palsgaard, T. Gunst, T. Markussen, K. Stokbro, M. Brandbyge, O. Hansen. "Interface band gap narrowing behind open circuit voltage losses in Cu<sub>2</sub>ZnSnS<sub>4</sub> solar cells". *Appl. Phys. Lett.* 110,083903 (2017). DOI: 10.1063/1.4976830.
- [49] M. Neuschitzer, K. Lienau, M. Guc, L. C. Barrio, S. Haass, J. M. Prieto, Y. Sanchez, M. Espindola-Rodriguez, Y. Romanyuk, A. Perez-Rodriguez. "Towards high performance Cd-free CZTSe solar cells with a ZnS(O,OH) buffer layer: the influence of thiourea concentration on chemical bath deposition. *J. Phys. D: Appl. Phys.* 49 125602 (2016). DOI: <https://doi.org/10.1088/0022-3727/49/12/125602>.
- [50] F. Liu, C. Yan, J. Huang, K. Sun, F. Zhou, J. A. Stride, M. A. Green and X. Hao. "Nanoscale microstructure and chemistry of Cu<sub>2</sub>ZnSnS<sub>4</sub>/CdS interface in kesterite Cu<sub>2</sub>ZnSnS<sub>4</sub> solar cells". *Adv. Energy Mater.* 6, (2016) 1600706. DOI:10.1002/aenm.201600706.